Accepted article: *J. Inorg. Biochem.* **2019**, *194*, 160-169.

Interactions of Acetamide and Acrylamide with Heme Models: Synthesis, Infrared Spectral, and Solid State Molecular Structures of Five- and Six-Coordinate Ferric Porphyrin Derivatives

Nan Xu,[a]* Ye Guan,[b] Nhi Nguyen,[a] Colin Lingafelt,[a] Douglas R. Powell,[b] and George B. Richter-Addo[b]*

[a] *Department of Chemistry, Pennsylvania State University Altoona, 3000 Ivyside Park, Altoona, Pennsylvania, U.S.A., 16601.*

[b] *Price Family Foundation Institute of Structural Biology, and Department of Chemistry and Biochemistry, University of Oklahoma, 101 Stephenson Parkway, Norman, Oklahoma, U.S.A., 73019.*

* *Corresponding author:*

(N. Xu) E-mail address: nxx103@psu.edu

(G. B. Richter-Addo) E-mail address: grichteraddo@ou.edu

Keywords: iron porphyrin, coordination, X-ray, acetamide, acrylamide, nitric oxide

ABSTRACT

The amide functional group is a fundamental building block of proteins, but is also present in several industrial chemicals such as acetamide and acrylamide. Some acetamide derivatives are known to deplete cytoplasmic heme, and some acrylamide derivatives are known to cause porphyria and may activate soluble guanylyl cyclase through a heme-dependent mechanism. We have prepared a representative set of six-coordinate acetamide and acrylamide (L) complexes of iron porphyrins of the form $[(por)Fe(L)_2]ClO_4$ (por = TPP (tetraphenylporphyinato dianion), T(*p*-OMe)PP (tetrakis(*p*-methoxyphenyl)porphyrinato dianion)) in 76–83% yields. We have also prepared the five-coordinate derivatives $[(OEP)Fe(L)]ClO_4$ (OEP = octaethylporphyrinato dianion) in 68–75% yields. These compounds were characterized by IR spectroscopy and by single-crystal X-ray crystallography. The molecular structures reveal the monodentate *O*-binding of the acetamide and acrylamide ligands to the ferric centers, with variable H-bonding exhibited between the acetamide/acrylamide $–NH_2$ moieties and the perchlorate anions. The five-coordinate OEP derivatives exhibit a π-π stacking of their porphyrin macrocycles, with the acetamide complex in the Class I and the acrylamide complex in the Class S groups. These compounds represent the first structurally characterized acetamide and acrylamide adducts of iron porphyrins. Reactions of the six-coordinate derivatives with NO result in the nitrosyl $[(por)Fe(NO)(L)]ClO_4$ derivatives that have been characterized by IR spectroscopy.

1. Introduction

The amide functional group –C(=O)N– is a very important one in biology. Not only does it serve as a building block in the assembly of the primary amino acid sequence of proteins, but it is also present in several organic derivatives of industrial and biological significance. Acetamide ($CH_3C(=O)NH_2$) and acrylamide ($CH_2=CHC(=O)NH_2$) are among the simplest 1° amides.

Acetamide is used as a solvent and in the plastics industry as a plasticizer, and is also present in red beetroot [1]. Acetamide derivatives such as haloacetamides have been identified as drinking water disinfection products (from wastewater disinfection processes) and there is an intense interest in their mechanism of formation and detoxification, as they are generally cytotoxic and genotoxic to mammalian cells [2]. Such haloacetamides are generated during the disinfection (by chloramines) of wastewater containing pharmaceuticals such as acetaminophen [3], or by the Fe-enabled decomposition of the antibiotic chloramphenicol [4]. Acrylamide is also widely used in the paper, plastics, and polymer industries. Acrylamide is neurotoxic to humans, and is categorized as a likely human carcinogen. Attention to the harmful effects of acrylamide increased when it was discovered to be present in some foods, particularly those that are cooked at high temperatures [5-7].

The interactions of acetamide and acrylamide derivatives with heme proteins have received some attention, but the available information is rather limited. In contrast, their coordination chemistry is quite well developed. They can bind to a variety of metals such as Fe, Co, Ni, Zn, Cr, Mn, Cu, Pd, and Pt through either the O-atom of the carbonyl group, the N-atom of the amide group, or the C=C double bond (of acrylamide) [8-17]. The monodentate *O*-binding mode appears to be heavily favored over the other two binding modes in these metal complexes. The sole *N*-binding mode in the tautomeric form has been shown in the crystal structure of the

bisacetamide complex *trans*-[$PtCl_2(HN{=}C(OH)Me)_2$] prepared by hydrolysis of its acetonitrile precursor [15]. In addition, a structure with two Pt atoms bridged by two acrylamides through the amidate N atoms and the C=C bond was proposed in an acrylamide platinum polymer based on its IR spectrum [16].

Importantly, allyl isopropyl acetamide is known, upon administration, to deplete cytoplasmic heme (via destruction of the cytochrome P450 heme) [18, 19]. *N,N*-methylene-bis-acrylamide is also known as a causative agent of anemia and porphyria in experimental animals [20]. Cytochrome P450 2E1 participates actively in acrylamide metabolism presumably through a Type I interaction [21, 22]. In a landmark 1982 study, Dawson et. al demonstrated that ferric cytochrome $P450_{CAM}$ in complex with *O*-donor ligands such as alcohols and amides (but not carboxylates or *N*-/*S*-donor ligands), displayed spectral properties similar to that of the ferric resting state of the enzyme; this provided strong evidence that the sixth axial ligand of cytochrome $P450_{CAM}$ was an *O*-bound ligand [23]. Interactions of the 3° amide *N,N*-dimethylformamide with synthetic ferric heme models have also been reported [24, 25]. Interestingly, it has been reported that an acrylamide derivative activates soluble guanylyl cyclase through a heme-dependent mechanism [26]. It is somewhat surprising, therefore, that not much is currently known about the interactions of acetamide and acrylamide and their derivatives with heme derivatives. The public awareness of acrylamide as a health hazard recently received a boost in the popular media when a judge in California ruled that coffee companies needed to label their hot-brewed coffee with acrylamide cancer warnings [27].

We thus aimed to explore the interactions of the parent acetamide and acrylamide compounds with heme models to help determine if such direct complexation was possible, and to define the nature of such interactions if they did occur. We recently reported the preparation of

such adduct formation with synthetic Mn porphyrins [28]. We have since extended this work to the more biologically relevant Fe porphyrins. In this article, we report the preparation, IR spectroscopic, and X-ray crystal structural characterization of several heme models with the parent acetamide and acrylamide. Further, we report on their reactivity with nitric oxide (NO) to yield *trans* nitrosyl-amide derivatives.

2. Experimental section

All reactions were performed under an atmosphere of prepurified nitrogen using standard Schlenk glassware and/or in an Innovative Technology Labmaster 100 Dry Box or a MBraun Unilab Glovebox. Solutions for spectroscopic studies were also prepared under a nitrogen atmosphere. Solvents were distilled from appropriate drying agents under nitrogen just prior to use: CH_2Cl_2 (CaH_2), hexane (CaH_2), toluene (Na).

2.1. Chemicals and instrumentation. Acetamide ($CH_3C(=O)NH_2$, >99%), acrylamide ($CH_2CHC(=O)NH_2$, >99%), $AgClO_4$ (97%), were purchased from Aldrich Chemical Company and used as received. Nitric oxide (98%, Matheson Gas) was passed through KOH pellets and a cold trap (dry ice/acetone) to remove higher nitrogen oxides. The $[(por)Fe(THF)_2]ClO_4$ (por = TPP (tetraphenylporphyinato dianion), T(*p*-OMe)PP (tetrakis(*p*-methoxyphenyl)porphyrinato dianion), and OEP (octaethylporphyrinato dianion)) precursors were prepared similarly to that used for the TPP derivative [29]. Infrared spectra were recorded on a Bio-Rad FT-155 FTIR spectrometer. A Bruker Vector 22 FTIR spectrometer equipped with a mid-IR fiber-optic dip probe and liquid nitrogen cooled MCT detector (RemSpec Corporation, Sturbridge, MA, USA) was used to monitor the reactions involving nitric oxide (NO) gas.

2.2. Preparation of complexes

[(TPP)Fe(O=C(NH$_2$)CH$_3$)$_2$]ClO$_4$. To a toluene solution (20 mL) of [(TPP)Fe(THF)$_2$]ClO$_4$ (14.8 mg, 0.017 mmol) was added CH_3CONH_2 (10 mg, 0.17 mmol). The mixture was stirred for 45 min, during which time the color of the solution changed from brown-purple to red-purple. The solvent was reduced to ~10 mL and hexane (30 mL) was added. The resulting solution was placed in a freezer (–22 ºC) overnight. The violet crystalline solid that formed was collected by filtration, washed with hexane (2×15 mL), and dried in vacuo to give [(TPP)Fe(CH_3CONH_2)$_2$]ClO$_4$ (0.011 g, 0.013 mmol, 76% isolated yield). Slow evaporation of a CH_2Cl_2/cyclohexane (4:1 ratio; 5 mL) solution of the product at room temperature gave suitable crystals for X-ray diffraction studies. IR (KBr, cm^{-1}): υ_{CO} 1661 m; also υ_{ClO_4} 1146 s, 1112 s, 1087 m, 627 m.

The other acetamide and acrylamide iron porphyrin complexes were generated similarly using the respective porphyrin macrocycles and amides:

[(TPP)Fe(O=C(NH$_2$)CH=CH$_2$)$_2$]ClO$_4$. Yield: 83%. IR (KBr, cm^{-1}): υ_{CO} 1653 m and 1648 m; also υ_{ClO_4} 1120 m, 1107 s, 1090 s, 1070 s, 625 m. Slow evaporation of a CH_2Cl_2/cyclohexane (3:1 ratio; 4 mL) solution of the product at room temperature gave suitable crystals for X-ray diffraction studies.

[(T(*p*-OMe)PP)Fe(O=C(NH$_2$)CH$_3$)$_2$]ClO$_4$. Yield: 79%. IR (KBr, cm^{-1}): υ_{CO} 1664 m and 1657 m; also υ_{ClO_4} 1113 m, 1107 s, 1083 s, 1062 s, 625 m. Slow evaporation of a CH_2Cl_2/cyclohexane/hexanes (3:1:1 ratio; 5 mL) solution of the product at room temperature gave suitable crystals for X-ray diffraction studies.

[(OEP)Fe(O=C(NH$_2$)CH$_3$)]ClO$_4$. Yield: 68%. IR (KBr, cm^{-1}): υ_{CO} 1655 m; also υ_{ClO_4} 1145 m, 1108 s, 1055 m, 624 m. Slow evaporation of a CH_2Cl_2/cyclohexane (3:1 ratio; 4 mL) solution of the product at room temperature gave suitable crystals for X-ray diffraction studies.

[(OEP)Fe(O=C(NH$_2$)CH=CH$_2$)]ClO$_4$. Yield: 75%. IR (KBr, cm^{-1}): υ_{CO} 1655 m; also υ_{ClO_4} 1146 m, 1104 s, 1056 m, 622 m. Slow evaporation of a CH_2Cl_2/cyclohexane (3:1 ratio; 4 mL) solution of the product generated suitable crystals for X-ray diffraction studies.

Preliminary reaction of [(TPP)Fe(O=C(NH$_2$)CH=CH$_2$)$_2$]ClO$_4$ with nitric oxide (NO). Nitric oxide was slowly bubbled through a CH_2Cl_2 solution (5 mL) of [(TPP)Fe(O=C(NH$_2$)CH=CH$_2$)$_2$]ClO$_4$ (18 mg, 0.020 mmol). During this time, the color of the solution changed from red-purple to bright red. A mixture of [(TPP)Fe(NO)(O=C(NH$_2$)CH=CH$_2$)]ClO$_4$ (~23%) and [(TPP)Fe(NO)]ClO$_4$ (~77%) was formed in the solution based on the infrared spectrum. IR (CH_2Cl_2, cm^{-1}): υ_{NO} 1919 m, υ_{CO} 1656 m for [(TPP)Fe(NO)(O=C(NH$_2$)CH=CH$_2$)$_2$]ClO$_4$; υ_{NO} 1849 m for [(TPP)Fe(NO)]ClO$_4$.

2.3 A note on sample purity

We frequently encounter non-reproducible elemental analyses for these and such [(por)Fe(L)$_2$]$^+$ complexes where L is a weakly bound ligand. This is due, in large part, to the frequent displacement of the ligands in these ferric complexes by H_2O (from lab moisture) and by our lack of effective control regarding how the subcontracted company handles its samples prior to their anaerobic/aerobic analyses. Mass spectral analyses also do not give us useful information regarding the identity of the cation-anion pair, with the [(por)Fe]$^+$ cations dominating the spectra. Consequently, we resort to X-ray crystallography to correctly identify these and related compounds. To check if the crystal structures obtained are representative of the

identities of the bulk samples, we record and compare the IR spectra of the crystals and the bulk samples. For the new complexes reported in this paper, the IR spectra of the crystals used for X-ray structure determinations match those of the bulk samples, providing confidence that the crystal structures are indeed representative of the identities of the bulk samples.

2.4. Solid-State Structural Determinations

Details of crystal data and refinement are given in Table 1. Single-crystal X-ray diffraction data were collected using an D8 diffractometer with a Bruker APEX ccd area detector [30, 31] with graphite-monochromated Mo Kα radiation (λ = 0.71073 Å). The structures were solved by direct methods and using the SHELXTL system and refined by full-matrix least-squares methods on F^2 [32].

(i) [(TPP)Fe(O=C(NH$_2$)CH$_3$)$_2$]ClO$_4$. The complex was located on an inversion center. The anion was located on a two-fold axis; the occupancies for the M and N groups refined to 0.329(6) and 0.171(6), respectively. Restraints on the positional and displacement parameters of the disordered atoms were required. Cell parameters were determined from a non-linear least squares fit of 5876 peaks in the range $2.72 < \theta < 28.31°$. A total of 28508 data were measured in the range $1.80 < \theta < 28.32°$ using ω oscillation frames. The data were corrected for absorption by the empirical method [33] giving minimum and maximum transmission factors of 0.813 and 0.962. The data were merged to form a set of 5138 independent data with R(int) = 0.0451 and a coverage of 100.0 %. The monoclinic space group *C*2/*c* was determined by systematic absences and statistical tests and verified by subsequent refinement. Non-hydrogen atoms were refined with anisotropic displacement parameters. Hydrogen atom positions were initially determined by geometry and refined by a riding model. Hydrogen atom displacement parameters were set to 1.2 times (1.5 for methyl) the displacement parameters of the bonded atoms. A total of 351

parameters were refined against 240 restraints and 5138 data to give wR(F^2) = 0.1061 and S = 1.010 for weights of w = 1/[$\sigma^2(F^2)$ + (0.0560 P)^2 + 5.0000 P], where P = [F_o^2 + 2F_c^2]/3. The final R(F) was 0.0392 for the 4442 observed, [$F > 4\sigma(F)$], data. The largest shift/s.u. was 0.007 in the final refinement cycle.

(ii) [(TPP)Fe(O=C(NH$_2$)CH=CH$_2$)$_2$]ClO$_4$·CH$_2$Cl$_2$. A cyclohexane solvent molecule was severely disordered and was best modeled using the *Squeeze* program [34]. Restraints on the N–H bond lengths and the displacement parameters of all atoms were required. Cell parameters were determined from a non-linear least squares fit of 4085 peaks in the range 2.46 < θ < 25.50°. A total of 15507 data were measured in the range 1.63 < θ < 25.56° using ω oscillation frames. The data were corrected for absorption by the empirical method [33] giving minimum and maximum transmission factors of 0.5673 and 0.7452. The data were merged to form a set of 9456 independent data with R(int) = 0.0450 and a coverage of 98.2 %. The triclinic space group $P\bar{1}$ was determined by statistical tests and verified by subsequent refinement. Non-hydrogen atoms were refined with anisotropic displacement parameters. Hydrogen atom positions were initially determined by geometry and refined by a riding model. Hydrogen atom displacement parameters were set to 1.2 times (1.5 for methyl) the displacement parameters of the bonded atoms. A total of 604 parameters were refined against 572 restraints and 9456 data to give wR(F^2) = 0.2356 and S = 1.011 for weights of w = 1/[$\sigma^2(F^2)$ + (0.1100 P)^2 + 2.2000 P], where P = [F_o^2 + 2F_c^2]/3. The final R(F) was 0.0819 for the 5161 observed, [$F > 4\sigma(F)$], data. The largest shift/s.u. was 0.002 in the final refinement cycle.

(iii) [(T(*p*-OMe)PP)Fe(O=C(NH$_2$)CH$_3$)$_2$]ClO$_4$. The crystal structure contained three sites of disordered CH_2Cl_2 solvent and were best modeled using the *Squeeze* program [34]. One aromatic ring and one methyl group were also disordered. The occupancies of the aromatic C35–C40 atoms

refined to 0.677(6) and 0.323(6) for the unprimed and primed atoms. The occupancies of acetamide C49 and C50 atoms refined to 0.581(11) and 0.419(11) for the unprimed and primed atoms. Restraints on the positional and displacement parameters of the disordered atoms were required. Cell parameters were determined from a non-linear least squares fit of 9644 peaks in the range $2.24 < \theta < 30.70°$. A total of 73900 data were measured in the range $1.110 < \theta < 31.502°$ using φ and ω oscillation frames. The data were corrected for absorption by the empirical method [33] giving minimum and maximum transmission factors of 0.898 and 0.963. The data were merged to form a set of 17174 independent data with R(int) = 0.0399 and a coverage of 100.0 %. The triclinic space group $P\ \bar{1}$ was determined by statistical tests and verified by subsequent refinement. Non-hydrogen atoms were refined with anisotropic displacement parameters. Hydrogen atom displacement parameters were set to 1.2 (1.5 for methyl) times the isotropic equivalent displacement parameters of the bonded atoms. A total of 693 parameters were refined against 276 restraints and 17174 data to give $wR(F^2) = 0.1103$ and S = 1.006 for weights of $w = 1/[\sigma^2(F^2) + (0.0520\ P)^2 + 0.5000\ P]$, where $P = [F_o^2 + 2F_c^2]/3$. The final R(*F*) was 0.0406 for the 12598 observed, $[F > 4\sigma(F)]$, data. The largest shift/s.u. was 0.003 in the final refinement cycle.

(iv) $[(OEP)Fe(O{=}C(NH_2)CH_3)]ClO_4{\cdot}(CH_2Cl_2)_2$. The solvent was disordered and refined with occupancies of 0.5. Restraints on the positional and displacement parameters of the disordered atoms were required. Restraints on the N5–H bond lengths were also required. Cell parameters were determined from a non-linear least squares fit of 9558 peaks in the range $2.20 < \theta < 28.32°$. A total of 29962 data were measured in the range $1.53 < \theta < 28.39°$ using ω oscillation frames. The data were corrected for absorption by the empirical method [33] giving minimum and maximum transmission factors of 0.743 and 0.872. The data were merged to form a set of 10797 independent data with R(int) = 0.0697 and a coverage of 99.9 %. The triclinic

space group $P\bar{1}$ was determined by statistical tests and verified by subsequent refinement. Non-hydrogen atoms were refined with anisotropic displacement parameters. Hydrogen atom positions were initially determined by geometry and refined by a riding model. Hydrogen atom displacement parameters were set to 1.2 (1.5 for methyl) times the displacement parameters of the bonded atoms. A total of 538 parameters were refined against 22 restraints and 10797 data to give wR(F^2) = 0.2038 and S = 1.010 for weights of w = 1/[$\sigma^2(F^2)$ + (0.1150 P)^2 + 0.3000 P], where P = [F_o^2 + 2F_c^2]/3. The final R(F) was 0.0731 for the 6979 observed, [$F > 4\sigma(F)$], data. The largest shift/s.u. was 0.001 in the final refinement cycle.

(v) [(OEP)Fe(O=C(NH$_2$)CH=CH$_2$)]ClO$_4$·CH$_2$Cl$_2$. Cell parameters were determined from a non-linear least squares fit of 5549 peaks in the range 2.43 < θ < 28.26°. A total of 27554 data were measured in the range 1.78 < θ < 28.26° using ω oscillation frames. The data were corrected for absorption by the empirical method [33] giving minimum and maximum transmission factors of 0.779 and 0.880. The data were merged to form a set of 9884 independent data with R(int) = 0.0392 and a coverage of 99.9 %. The monoclinic space group $P2_1/n$ was determined by systematic absences and statistical tests and verified by subsequent refinement. Non-hydrogen atoms were refined with anisotropic displacement parameters. Hydrogen atom positions of hydrogens bonded to carbons were initially determined by geometry and refined by a riding model. Hydrogen atom displacement parameters were set to 1.2 (1.5 for methyl) times the displacement parameters of the bonded atoms. A total of 493 parameters were refined against 9884 data to give wR(F^2) = 0.1103 and S = 1.006 for weights of w = 1/[$\sigma^2(F^2)$ + (0.0610 P)^2 + 0.8600 P], where P = [F_o^2 + 2F_c^2] /3. The final R(F) was 0.0402 for the 7920 observed, [$F > 4\sigma(F)$], data. The largest shift/s.u. was 0.001 in the final refinement cycle.

The crystallographic data for the complexes are summarized in Table 1.

3. Results and discussion

3.1. Preparation of complexes

Acetamide and acrylamide displace the bound THF ligands in the precursor ferric compounds $[(por)Fe(THF)_2]ClO_4$ (por = TPP, T(*p*-OMe)PP) in toluene solution at room temperature (~19 °C) to generate the bis-liganded $[(por)Fe(L)_2]ClO_4$ derivatives as shown in eq. 1. In the case where the OEP macrocycle is used, the five-coordinate $[(OEP)Fe(L)]ClO_4$ derivative is obtained (eq. 2)

$$[(por)Fe(THF)_2]ClO_4 + \text{xs. L} \rightarrow [(por)Fe(L)_2]ClO_4 + 2\ THF \qquad (1)$$

L = acetamide; por = TPP (76%), T(*p*-OMe)PP (79%)
L = acrylamide; por = TPP (83%)

$$[(OEP)Fe(THF)_2]ClO_4 + \text{xs. L} \rightarrow [(OEP)Fe(L)]ClO_4 + 2\ THF \qquad (2)$$

L = acetamide (68%), acrylamide (75%)

These red-purple and moderately air-stable solid products are obtained in good isolated yields after workup. We used excess amides in the reactions, as these amide ligands dissociate from the Fe centers in solution at low concentrations in the absence of added ligand.

The IR spectra of the ferric bis-acetamide complexes $[(TPP)Fe(O=C(NH_2)CH_3)_2]ClO_4$ and $[(T(p\text{-OMe})PP)Fe(O=C(NH_2)CH_3)_2]ClO_4$ as KBr pellets show bands at 1661 cm^{-1} and 1653/1648 cm^{-1}, respectively, assigned the υ_{CO} of the bound acetamides. These bands are lower than those reported for matrix-isolated acetamide (1726 cm^{-1}) [35] or acetamide in the solid state (1695 cm^{-1}; the υ_{CO} band of free acrylamide has been determined to be mixed with contributions from $\upsilon_{C=C}$ and δ_{NH_2}). [36, 37]. The isolated mono-amide derivative

[(OEP)Fe(O=C(NH_2)CH_3)]ClO_4 displays a band at 1655 cm^{-1} in its IR spectrum assigned to υ_{CO}.

The IR spectra of the related bis-acrylamide [(TPP)Fe(O=C(NH_2)CH=CH_2)$_2$]ClO_4 and mono-acrylamide [(OEP)Fe(O=C(NH_2)CH=CH_2)]ClO_4 derivatives reveal bands at 1653/1648 cm^{-1} and 1655 cm^{-1}, respectively, assigned to υ_{CO} of the bound ligands. These bands are similar to those observed for the acetamide derivatives, and are lower than that reported for free acrylamide in the solid state (1681 cm^{-1}) [36]. Such a lowering of the υ_{CO} of bound amides, for both acetamide and acrylamide, upon coordinated to metal ions is normally associated with the *O*-binding mode of these ligands. To determine if this is indeed the case, we sought to determine the X-ray crystal structures of these compounds to unambiguously establish the amide binding modes to the heme model centers.

3.2. Crystallography

X-ray diffraction quality crystals of three bis-amide and two mono-amide derivatives were obtained by slow evaporation from their CH_2Cl_2/cyclohexane solutions in the presence of excess amide.

3.2.1. The six-coordinate bis-amide complexes: The structures of the acetamide complexes [(TPP)Fe(O=C(NH_2)CH_3)$_2$]ClO_4 and [(T(*p*-OMe)PP)Fe(O=C(NH_2)CH_3)$_2$]ClO_4, and the acrylamide complex [(TPP)Fe(O=C(NH_2)CH=CH_2)$_2$]ClO_4 are shown in Figures 1, 3 and 4, respectively, with selected bond lengths listed in Table 2.

The structure of the acetamide complex [(TPP)Fe(O=C(NH_2)CH_3)$_2$]ClO_4 (Figure 1) reveals a clear monodentate *O*-binding mode of both axial acetamide ligands to the central Fe atom, with a H-bonding interaction between one of the H-atoms of the acetamide –NH_2 group

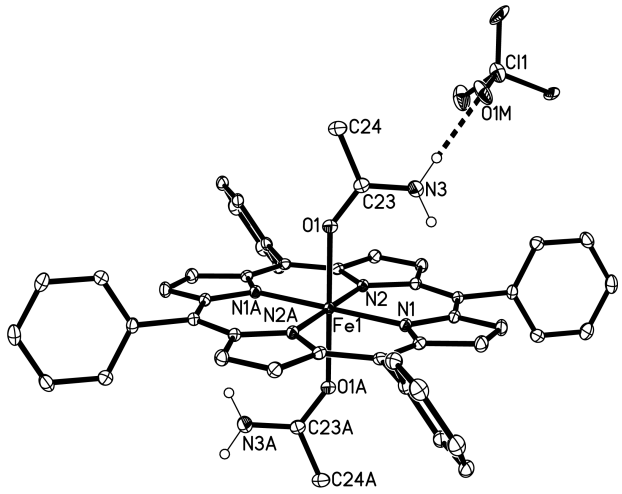

Figure 1. The structure of the six-coordinate acetamide complex $[(TPP)Fe(O=C(NH_2)CH_3)_2]ClO_4$. Both axial acetamide $–NH_2$ groups are involved in such H-bonding with the perchlorate counteranions. Hydrogen atoms attached to carbon atoms have been omitted for clarity.

and an O-atom of the perchlorate anion (N3···O1M = 2.82 Å); both axial acetamide $–NH_2$ groups are involved in such H-bonding with the perchlorate counteranions in the crystal (not shown). In this complex, the acetamide ligand is planar and is oriented essentially perpendicular (~73°) to the 24-atom mean porphyrin plane. The acetamide core Fe–O–C–N framework is in the *syn* conformation for both ligands, with a torsion angle of –14.6(3)°. The Fe–N(por) bond lengths of 2.0459(14) and 2.0477(13) Å in $[(TPP)Fe(O=C(NH_2)CH_3)_2]ClO_4$ (Figure 1) are typical of those determined for six-coordinate high-spin ferric porphyrins (~2.045 Å) [38]. Not surprisingly, the Fe atom sits essentially in the 24-atom porphyrin plane.

The *O*-binding mode of acetamide in $[(TPP)Fe(O=C(NH_2)CH_3)_2]ClO_4$ (Figure 1) is consistent with the observed lowering of the υ_{CO} band in its IR spectrum when compared with the υ_{CO} of the free ligand, and suggests a contribution of the resonance form **B** in this complex (Figure 2) with a slightly less than C=O double-bond character [39]. Also consistent with this

view is that the C–O bond length in [(TPP)Fe(O=C(NH_2)CH_3)$_2$]ClO_4 at 1.251(3) Å is slightly longer than that reported for free acetamide (1.2419(17) Å) [40].

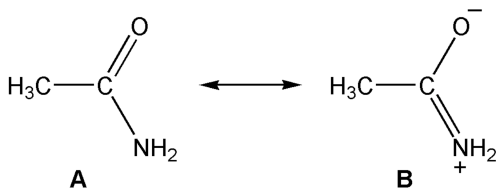

Figure 2. Resonance contributions of the acetamide ligand.

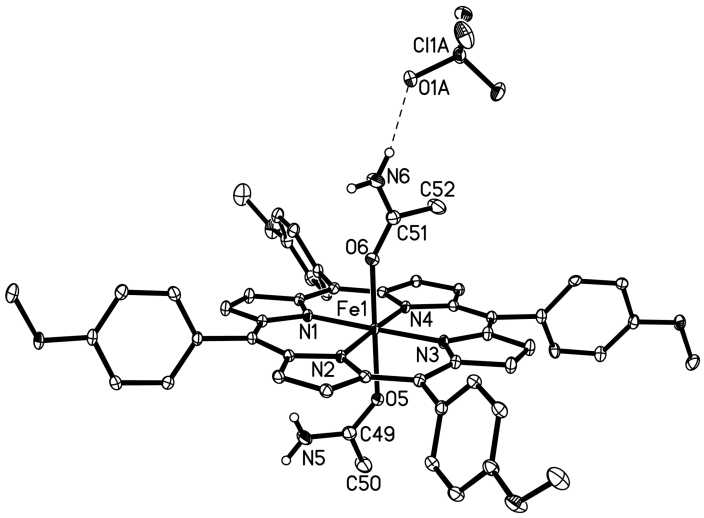

Figure 3. The structure of the six-coordinate acetamide complex [(T(*p*-OMe)PP)Fe(O=C(NH_2)CH_3)$_2$]-ClO_4. Only one component of the disordered C49 and C50 atoms is shown. Hydrogen atoms attached to carbon atoms have been omitted for clarity.

The structure of the T(*p*-OMe)PP analog (Figure 3) is similar to that of the TPP derivative in many respects. The planar *O*-bound acetamide is essentially perpendicular (~88°) to the 24-atom mean porphyrin plane, and makes a H-bonding contact with the perchlorate anion (N6···O1A = ~2.89 Å), although in this derivative, only one of the axial acetamides is involved in this H-bonding interaction with the counteranion in the crystal. Further, although the core Fe–

O–C–N framework for the acetamide (with H-bonding contact with perchlorate) is in the *anti* conformation (torsion angle of –178°), the second axial acetamide without a H-bonding interaction with the anion is in the *syn* conformation (torsion angle of –25°). The observation of generally longer C–O and shorter C–N bond lengths of the bound acetamides in these metalloporphyrin derivatives (Table 2) are consistent with those observed for other *O*-bound acetamides in coordination complexes of Pd [10], Pt [14], and Ni [41], although on occasion such bond length changes are not so distinct (e.g., for a Mn derivative) [42] or are reversed (for a hexanuclear Fe complex [9]).

The structure of the acrylamide complex $[(TPP)Fe(O=C(NH_2)CH=CH_2)_2]ClO_4$ is shown in Figure 4, with selected bond lengths listed in Table 2. The *O*-bonded acrylamide

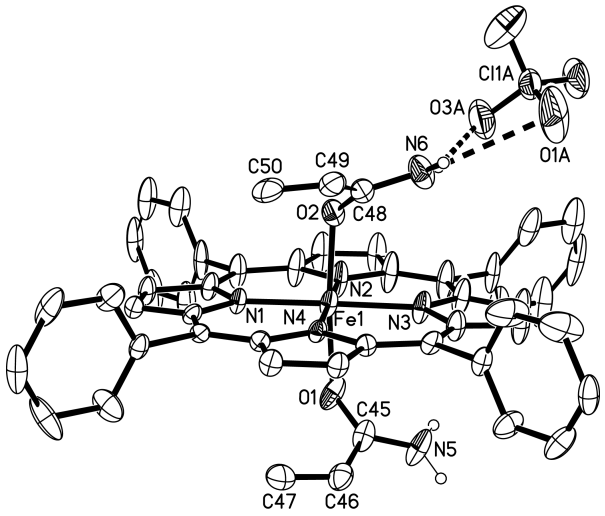

Figure 4. The structure of the six-coordinate acrylamide complex $[(TPP)Fe(O=C(NH_2)CH=CH_2)_2]ClO_4$. Hydrogen atoms attached to carbon atoms have been omitted for clarity.

is clearly observed in this structure for both nearly planar acrylamide ligands (largest deviations from planarity of ~0.1 Å for the C46 and C49 atoms. Both axial acrylamide ligands are in the

Fe–O–C–N *syn* conformation, and the ligand engages in H-bonding interactions with the perchlorate anion in the crystal. Interestingly, the acrylamide ligand planes are "bent" with respect to the porphyrin plane, with interplanar angles of ~34°. This places the C=C moieties of the ligands at almost parallel orientations (~4°) with the porphyrin plane that is now only a relatively short ~3.2 Å distance away.

O-bonded acrylamide ligands in coordination compounds are proposed to have contributions from the resonance forms shown in Figure 5 [8]. The expected conjugation

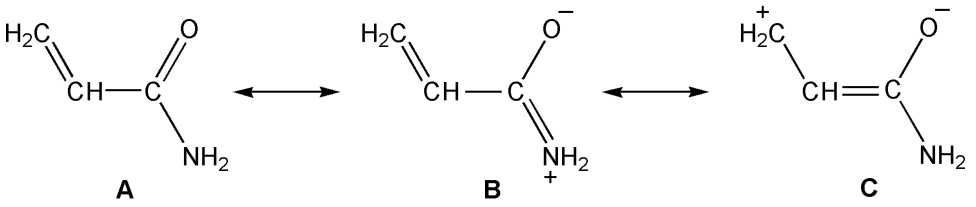

Figure 5. Resonance contributions of acrylamide

along the acrylamide backbone thus makes it challenging to interpret subtle changes in bond lengths and angles within the acrylamide backbone with confidence. For example, while the C=O bond lengths of 1.262(6) and 1.268(7) Å in $[(TPP)Fe(O=C(NH_2)CH=CH_2)_2]ClO_4$ (Figure 4, and its Mn analog in Table 2) are longer than the C=O bond length in free acrylamide (1.2413(14) Å) [43] (a similar lengthening has been observed in coordination complexes of Mn [11], Cu [13], and Co [12]) the C–N bond lengths of 1.320(7) and 1.336(7) Å are not significantly different from that of free acrylamide (1.3275(14) Å) [43].

3.2.2. The five-coordinate complexes: The OEP derivatives of acetamide and acrylamide crystallized as their five-coordinate forms. The X-ray crystal structures of the acetamide

complex $[(OEP)Fe(O=C(NH_2)CH_3)]ClO_4$ and acrylamide complex $[(OEP)Fe(O=C(NH_2)CH=CH_2)]ClO_4$ are shown in Figures 6 and 7, respectively.

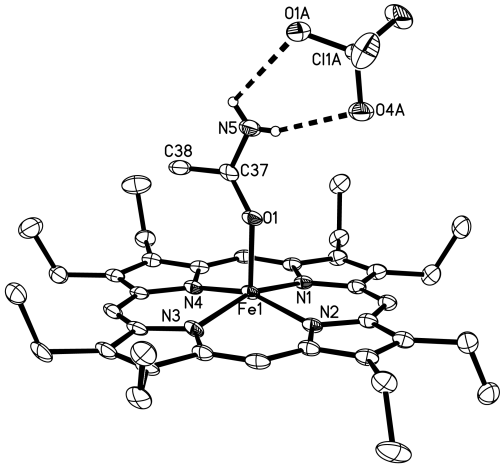

Figure 6. The structure of the five-coordinate acetamide complex $[(OEP)Fe(O=C(NH_2)CH_3)]ClO_4$. Hydrogen atoms attached to carbon atoms have been omitted for clarity. Not shown is the π-π stacking of adjacent OEP macrocycles.

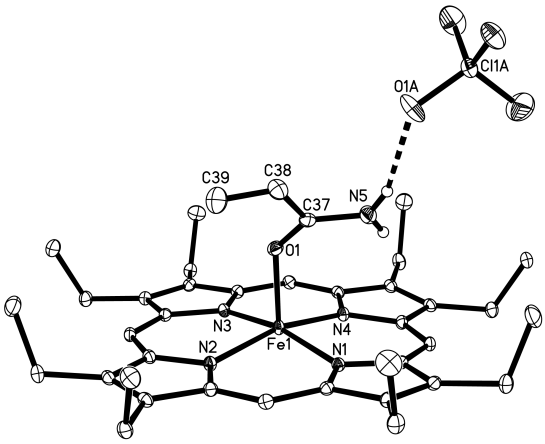

Figure 7. The structure of the five-coordinate acrylamide complex $[(OEP)Fe(O=C(NH_2)CH=CH_2)]ClO_4$. Hydrogen atoms attached to carbon atoms have been omitted for clarity. Not shown is the π-π stacking of adjacent OEP macrocycles (see Figure 8).

In the acetamide complex [(OEP)Fe(O=C(NH_2)CH_3)]ClO_4, the equatorial Fe–N(por) and axial Fe–O bond lengths are 2.032(3)–2.039(3) Å and 1.962(2) Å, respectively. The central Fe atom is displaced 0.36 Å out of the 24-atom mean plane of the porphyrin ligand towards the acetamide ligand; such displacement of Fe towards the ligand is not uncommon in five-coordinate porphyrins. The acetamide C–O bond and C–N bond lengths are comparable to those observed in the six-coordinate TPP and T(*p*-OMe)PP derivatives described above. The Fe–O–C–N linkage is in the *anti* conformation (torsion angle of –170°), and the acetamide ligand plane nearly perpendicular to the porphyrin plane (84.2°). As observed with the six-coordinate analogs, the acetamide $–NH_2$ group similarly engages in a H-bonding interaction with the perchlorate anion (N5···O1A = 2.90 Å, N5···O4A = 3.01 Å).

The Fe atom in the five-coordinate acrylamide complex (Figure 7) is displaced by 0.26 Å towards the 24-atom mean porphyrin plane towards the ligand. The acrylamide ligand plane is oriented ~49° to the porphyrin plane with an Fe–O–C bond angle of 136.1(1)°. This observed interplanar angle of 49° is larger for the OEP derivative than what was observed in the six-coordinate TPP derivative (~34°, Figure 4), and may be facilitated by the observation that all eight porphyrin Et substituents in the OEP derivative point in the direction of the ligand. This view of minimizing a steric clash is consistent with the observation that the distance between the acrylamide C=C bond and the porphyrin plane is ~ 4.0 Å, which is ~0.8 Å longer than observed in the TPP analog.

Not shown in Figures 6 and 7 are the intermolecular π-π interactions between adjacent OEP macrocycles. This π-π stacking interaction is illustrated in Figure 8 for the acrylamide derivative, and its presence is consistent with the isolation of the stable five-coordinate complexes in crystalline form. Similar π-π interaction has been reported previously for a few

other five-coordinate (OEP)Fe derivatives [44-46] and the related Mn-acrylamide analog of this work [28].

As shown in Figures 8 and 9 for the five-coordinate [(OEP)Fe(O=C(NH_2)CH=CH_2)]-ClO_4, the mean plane separation (M.P.S.) between the adjacent 24-atom porphyrin planes is 3.3 Å. The Fe–Fe distance between adjacent cations is 4.1 Å with a lateral shift of ~1.6 Å (Figure 9).

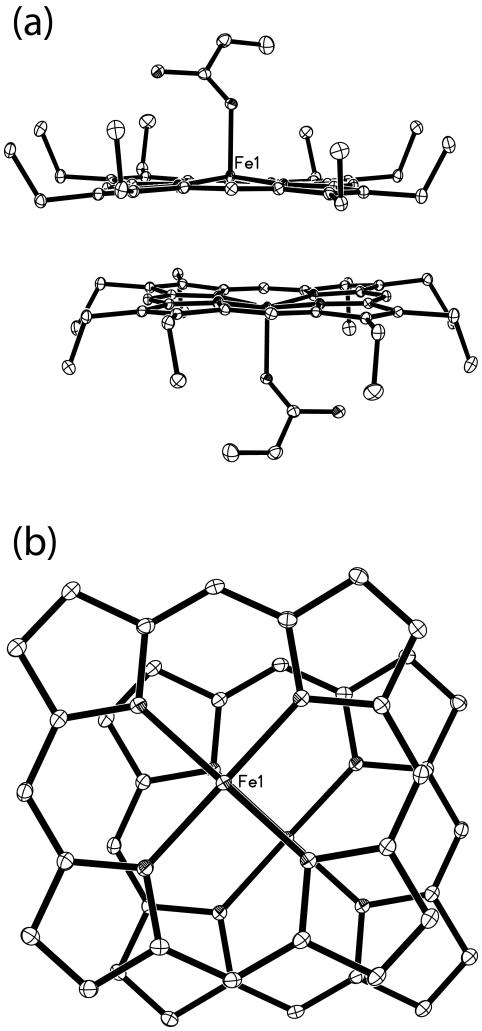

Figure 8. View of the π-π stacking involving the cation of [(OEP)Fe(O=C(NH_2)CH=CH_2)]ClO_4, showing (top) the 3.3 Å separation of the porphyrin planes, and (b) the slippage of the porphyrin rings relative to each other. Perchlorate anions and hydrogen atoms have been omitted for clarity.

This π-π stacking interaction, combined with the magnitudes of the M.P.S. and the lateral shift, places this compound in Class S with a strong π-π interaction, according to the nomenclature of Scheidt and Lee [47]. The acetamide OEP derivative in Figure 6 has a similar M.P.S (3.4 Å), but a longer Fe–Fe distance (5.0 Å) and lateral shift (2.9 Å). These measurements are closer to the compounds in Class I with an intermediate π-π interaction.

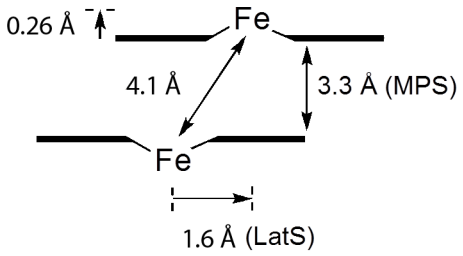

Figure 9. Sketch of the geometric parameters for the OEP-OEP π stacking in [(OEP)Fe(O=C(NH_2)-$CH=CH_2$)]ClO_4.

3.3. Reactions with NO gas

As mentioned earlier, the bis-amide complexes $[(por)Fe(amide)_2]^+$ are prone to axial ligand dissociation in solution. We thus sought to take advantage of this to prepare the ferric six-coordinate nitrosyl derivatives $[(por)Fe(NO)(amide)]^+$ by addition of NO to the precursors in solution. The reaction of the bis-acrylamide complex [(TPP)Fe(O=C(NH_2)$CH=CH_2$)$_2$]ClO_4 in CH_2Cl_2, in the presence of excess acrylamide, with NO gas results in the immediate formation of new bands in the IR spectrum at 1919 cm^{-1} and 1849 cm^{-1} (Figure 10), and an enhancement of the band at 1691 cm^{-1} (for free acrylamide, indicating its dissociation) and a decrease in intensity of the band at 1657 cm^{-1} (coordinated acrylamide) that is now shifted by ~2 cm^{-1} to 1655 cm^{-1} likely due to the replacement of the initially *trans* acrylamide with NO.

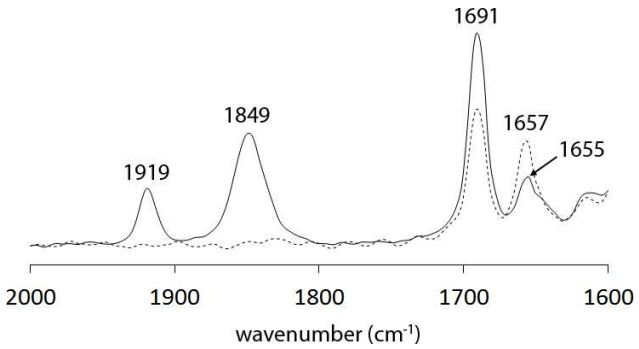

Figure 10. IR spectra of the starting $[(TPP)Fe(O=C(NH_2)CH=CH_2)_2]ClO_4$ complex (dashed line trace) and the mixture after the NO bubbling (solid line trace) in CH_2Cl_2 at room temperature.

We assign the bands at 1919 cm^{-1} and 1849 cm^{-1} to the υ_{NO}'s of the six-coordinate nitrosyl $[(TPP)Fe(NO)(O=C(NH_2)CH=CH_2)]ClO_4$ and the five-coordinate nitrosyl $[(TPP)Fe(NO)]ClO_4$, respectively. The lower band at 1849 cm^{-1} in the IR spectrum (Figure 10) is essentially identical to the 1848 cm^{-1} band observed for electrogenerated five-coordinate complex $[(TPP)Fe(NO)]ClO_4$ in CH_2Cl_2 [48].

The observed 1919 cm^{-1} band is similar to those reported for other ferric nitrosyl porphyrins with neutral *O*-bonded ligands *trans* to the axial NO, including the electrogenerated $[(TPP)Fe(NO)(L)]^+$ (L = dmso (1917 cm^{-1}), dimethylacetamide (1919 cm^{-1}), THF (1920 cm^{-1}), and DMF (1921 cm^{-1})) [48], and the isolated compounds $[(TPP)Fe(NO)(H_2O)]OTf$ (υ_{NO} 1897 cm^{-1}; KBr) [49], $[(TPP)Fe(NO)(H_2O)]ClO_4$ (υ_{NO} 1937 cm^{-1}; KBr) [50], and $[(TPP)Fe(NO)(HO\text{-}i\text{-}C_5H_{11})]ClO_4$ (υ_{NO} 1935 cm^{-1}; KBr) [51]. The IR data strongly suggests that the *O*-binding mode of the acrylamide is retained in the nitrosyl acetamide $[(TPP)Fe(NO)(O=C(NH_2)CH=CH_2)]ClO_4$ derivative.

Unfortunately, we have not been successful to date in crystallizing the six-coordinate nitrosyl acrylamide complex for a structure determination, nor have we been able to crystallize the other [(por)Fe(NO)(acetamide/acrylamide)]$^{+}$ derivatives from this work.

4. Conclusions

We have prepared a representative set of primary amide adducts of synthetic iron porphyrins from the reactions of the cationic [(por)Fe(THF)$_2$]ClO$_4$ precursors in toluene with acetamide or acrylamide. We have shown by IR spectroscopy that the C=O vibrations of the amides shift to lower energies upon the coordination, suggesting the *O*-binding mode of the ligands. This *O*-binding mode of the amides has been confirmed by the determination of the X-ray crystal structures of three six-coordinate [(TPP)Fe(O=C(NH$_2$)R)$_2$]ClO$_4$ compounds and two five-coordinate [(OEP)Fe(O=C(NH$_2$)R)]ClO$_4$ derivatives. We have shown that the core Fe–O–C–N linkage is present in either the *syn* or *anti* conformation depending on the complex. Importantly, this class of compounds represents the first reported structurally characterized examples of iron porphyrins complexed with primary amide ligands. Given the observations that an acrylamide derivative can activate soluble guanylyl cyclase in a heme-dependent manner [23], and that exposure of humans to industrial amides is a rising health concern, our structural work reported here thus represents an additional starting point for on-going structure-function studies involving the direct heme-amide interaction.

Supporting Information Available: CCDC 1847501–1847504 and 1847508 contain the supplementary crystallographic data for this paper. These data can be obtained free of charge via www.ccdc.cam.ac.uk/data_request/cif, or by emailing data_request@ccdc.cam.ac.uk, or by

contacting The Cambridge Crystallographic Data Centre, 12, Union Road, Cambridge CB2 1EZ, UK; fax: +44 1223 336033.

Acknowledgments

We are grateful for funding from U.S. National Science Foundation (CHE-1213674 and CHE-1566509 to G.B.R.A.) and RDG and MNS-SSRG funding from Penn State Altoona (to NX) for this work. The authors thank the National Science Foundation (CHE-0130835) and the University of Oklahoma for funds to purchase of the X-ray diffractometer and computers.

References

[1] Human Metabolome Database; http://www.hmdb.ca/metabolites/HMDB0031645.

[2] M.J. Plewa, M.G. Muellner, S.D. Richardson, F. Fasanot, K.M. Buettner, Y.T. Woo, A.B. Mckague, E.D. Wagner, Occurrence, synthesis, and mammalian cell cytotoxicity and genotoxicity of haloacetamides: An emerging class of nitrogenous drinking water disinfection byproducts, Environ. Sci. Technol., 42 (2008) 955-961.

[3] S.K. Ding, W.H. Chu, T. Bond, Q. Wang, N.Y. Gao, B. Xu, E.D. Du, Formation and estimated toxicity of trihalomethanes, haloacetonitriles, and haloacetamides from the chlor(am)ination of acetaminophen, J. Haz. Mater., 341 (2018) 112-119.

[4] W.H. Chu, S.K. Ding, T. Bond, N.Y. Gao, D.Q. Yin, B. Xu, Z.Q. Cao, Zero valent iron produces dichloroacetamide from chloramphenicol antibiotics in the absence of chlorine and chloramines, Water Res., 104 (2016) 254-261.

[5] L.A. Mucci, K.A. Wilson, Acrylamide intake through diet and human cancer risk, J. Agric. Food Chem., 56 (2008) 6013-6019.

[6] E. Tareke, P. Rydberg, P. Karlsson, S. Eriksson, M. Tornqvist, Acrylamide: A cooking carcinogen?, Chem Res Toxicol, 13 (2000) 517-522.

[7] O.E. Adedipe, S.D. Johanningsmeier, V.D. Truong, G.C. Yencho, Development and validation of a near-infrared spectroscopy method for the prediction of acrylamide content in French-fried potato, J. Agric. Food Chem., 64 (2016) 1850-1860.

[8] K.B. Girma, V. Lorenz, S. Blaurock, F.T. Edelmann, Coordination chemistry of acrylamide, Coord. Chem. Rev., 249 (2005) 1283-1293.

[9] C.P. Raptopoulou, A.K. Boudalis, Y. Sanakis, V. Psycharis, J.M. Clemente-Juan, M. Fardis, G. Diamantopoulos, G. Papavassillou, Hexanuclear iron(III) salicylaldoximato complexes presenting the $[Fe_6(\mu_3\text{-}O)_2(\mu_2\text{-}OR)_2]^{12+}$ core: Syntheses, crystal structures, and spectroscopic and magnetic characterization, Inorg. Chem., 45 (2006) 2317-2326.

[10] M. Broring, C. Kleeberg, A. Scheja, Cationic palladium(II) complexes of the sterically hindered bis(4-methylthiazolyl)isoindoline (4-Mebti) with neutral group XVI donor ligands, Inorg. Chim. Acta, 374 (2011) 572-577.

[11] K.B. Girma, V. Lorenz, S. Blaurock, F.T. Edelmann, Coordination chemistry of acrylamide 2. Classical complexes of acrylamide with manganese(II), iron(II) and nickel(II) chlorides: Syntheses and crystal structures, Z. Anorg. Allg. Chem., 631 (2005) 2763-2769.

[12] K.B. Girma, V. Lorenz, S. Blaurock, F.T. Edelmann, Coordination chemistry of acrylamide. 5. Crystal structures of complexes of metal(II) perchlorates and tetrafluoroborates with acrylamide, Z. Anorg. Allg. Chem., 632 (2006) 1874-1878.

[13] K.B. Girma, V. Lorenz, S. Blaurock, F.T. Edelmann, Coordination chemistry of acrylamide 3: Synthesis, crystal structure and IR spectroscopic properties of dichloro-tetrakis(*O*-acrylamide)copper(II), $[Cu(O\text{-}OC(NH_2)CH{=}CH_2)_4Cl_2]$, Inorg. Chim. Acta, 359 (2006) 364-368.

[14] R. Cini, F.P. Intini, L. Maresca, C. Pacifico, G. Natile, Isomerism of amides coordinated to platinum; X-ray crystal structure of *O*-bonded acetamide in a platinum(II) complex, Eur. J. Inorg. Chem., (1998) 1305-1312.

[15] R. Cini, F.P. Fanizzi, F.P. Intini, G. Natile, C. Pacifico, Isomerism of amides coordinated to platinum. X-ray crystal structure of dichloro-bisacetamide-platinum(II), Inorg. Chim. Acta, 251 (1996) 111-118.

[16] G. Schmuckler, B. Limoni, Interaction of platinum chloride with a polyacrylamide-gel and its monomeric analogs, J. Inorg. Nucl. Chem., 39 (1977) 137-141.

[17] K.B. Girma, V. Lorenz, S. Blaurock, F.T. Edelmann, Coordination chemistry of acrylamide 6: Formation and structural characterization of $[Fe(\textit{O}\text{-}OC(NH_2)CH{=}CH_2)_6][Fe_2OCl_6]$, Inorg. Chim. Acta, 361 (2008) 346-348.

[18] R. Fagard, C. Guguenguillouzo, The effect of hemin and of allyl isopropyl acetamide on protein-synthesis in rat hepatocytes, Biochem. Biophys. Res. Commun., 114 (1983) 612-619.

[19] F.D. Matteis, Loss of haem in rat liver caused by porphyrogenic agent 2-allyl-2-isopropylacetamide, Biochem. J., 124 (1971) 767-777.

[20] K. Hashimoto, J. Sakamoto, Anemia and porphyria caused by *N,N'*-methylene-bis-acrylamide (MBA) in mice and rats, Arch. Toxicol., 50 (1982) 47-55.

[21] S.C.J. Sumner, T.R. Fennell, T.A. Moore, B. Chanas, F. Gonzalez, B.I. Ghanayem, Role of cytochrome P450 2E1 in the metabolism of acrylamide and acrylonitrile in mice, Chem. Res. Toxicol., 12 (1999) 1110-1116.

[22] O. Doroshyenko, U. Fuhr, D. Kunz, D. Frank, M. Kinzig, A. Jetter, Y. Reith, A. Lazar, D. Taubert, J. Kirchheiner, M. Baum, G. Eisenbrand, F.I. Berger, D. Bertow, A. Berkessel, F. Sorgel, E. Schomig, D. Tomalik-Scharte, In vivo role of cytochrome P450 2E1 and glutathione-*S*-transferase activity for acrylamide toxicokinetics in humans, Cancer Epidem. Biom. Prev., 18 (2009) 433-443.

[23] J.H. Dawson, L.A. Andersson, M. Sono, Spectroscopic investigations of ferric cytochrome P45-CAM ligand complexes. identification of the ligand *trans* to cysteinate in the native enzyme, J. Biol. Chem., 257 (1982) 3606-3617.

[24] L.A. Bottomley, K.M. Kadish, Counterion and solvent effects on the electrode-reactions of iron porphyrins, Inorg. Chem., 20 (1981) 1348-1357.

[25] A. Chaudhary, R. Patra, S.P. Rath, Synthesis, structure and properties of a high-spin Fe(III) porphyrin with non-equivalent axial ligands: Implications for the hemoproteins, Indian J. Chem., Section A, 50 (2011) 432-437.

[26] M. Nakane, T. Kolasa, R.J. Chang, L.N. Miller, R.B. Moreland, J.D. Brioni, Acrylamide analog as a novel nitric oxide-independent soluble guanylyl cyclase activator, J. Pharmacol. Sci., 102 (2006) 231-238.

[27] E. Rosenberg, Coffee must carry cancer warning, California judge rules, The Washington Post, March 29, 2018. https://www.washingtonpost.com/news/to-your-health/wp/2018/2003/2029/coffee-must-carry-cancer-warning-california-judge-rules/?utm_term=.2091ac87454bb87453.

[28] N. Xu, A.W. Bevak, B.R. Armstrong, D.R. Powell, Synthesis, characterization and solid state molecular structures of five- and six-coordinate primary amide manganese porphyrin complexes, Polyhedron, 127 (2017) 432-437.

[29] L. Chen, G.-B. Yi, L.-S. Wang, U.R. Dharmawardana, A.C. Dart, M.A. Khan, G.B. Richter-Addo, Synthesis, characterization, and molecular structures of diethylnitrosamine metalloporphyrin complexes of iron, ruthenium, and osmium, Inorg. Chem., 37 (1998) 4677-4688.

[30] APEX2, Data Collection: APEX2 software reference manual, Bruker-AXS, Madison, WI, 2007.

[31] SAINT: Data Reduction and Correction Program, Data Reduction: SAINT software reference manual. Bruker-AXS, Madison, WI. , (2007).

[32] G.M. Sheldrick, Crystal Structure Refinement with *SHELXL*, Acta Cryst., C71 (2015) 3-8.

[33] L. Krause, R. Herbst-Irmer, G.M. Sheldrick, D. Stalke, Comparison of silver and molybdenum microfocus X-ray sources for single-crystal structure determination, J. Appl. Cryst., 48 (2015) 3-10.

[34] A.L. Spek, PLATON SQUEEZE: A tool for the calculation of the disordered solvent contribution to the calculated structure factors, Acta Cryst., C71 (2015) 9-18.

[35] R. Knudsen, O. Sala, Y. Hase, A low-temperature matrix-isolation infrared study of acetamides.1: Acetamide and some deuterated derivatives, J. Mol. Struc., 321 (1994) 187-195.

[36] J. Neville, The infrared and raman spectra and structure of acrylamide, J. Mol. Spectrosc., 6 (1961) 205-214.

[37] N. Sundaraganesan, N. Puviarasan, S. Mohan, Vibrational spectra, assignments and normal coordinate calculation of acrylamide, Talanta, 54 (2001) 233-241.

[38] W.R. Scheidt, C.A. Reed, Spin-state/stereochemical relationships in iron porphyrins: Implications for the hemoproteins, Chem. Rev., 81 (1981) 543-555.

[39] H. Sigel, R.B. Martin, Coordinating properties of the amide bond. stability and structure of metal ion complexes of peptides and related ligands, Chem. Rev., 82 (1982) 385-426.

[40] J.W. Bats, M.C. Haberecht, M. Wagner, A new refinement of the orthorhombic polymorph of acetamide, Acta Cryst. E, 59 (2003) O1483-O1485.

[41] M.E. Stone, B.E. Robertson, E. Stanley, Crystal Structures of Dichlorotetrakis(acetaldoxime)nickel(II) and tetrakis(acetamide)bisaquonickel(II) dichloride, J. Chem. Soc. A, Inorg. Phys. Theor., (1971) 3632-3636.

[42] J.-L. Du, S.J. Rettig, R.C. Thompson, J. Trotter, P. Betz, A. Bino, Structure and magnetic properties of monophenylphosphinate bridged chain polymers of manganese(II), $[MnL_2(HPhPO_2)_2]X$ (where L = $HPhPO_2H$, CH_3CONH_2, H_2O, $HCONH(CH_3)$, and C_5H_5N), Can. J. Chem., 70 (1992) 732-741.

[43] Q.L. Zhou, Z.H. Zhang, Z.L. Jing, Acrylamide, Acta Cryst. E, 63 (2007) O3039-U3433.

[44] N. Xu, L. Goodrich, N. Lehnert, D.R. Powell, G.B. Richter-Addo, Five- and six-coordinate adducts of nitrosamines with ferric porphyrins: Structural models for the Type II interactions of nitrosamines with ferric cytochrome P450, Inorg. Chem., 49 (2010) 4405-4419.

[45] E.G. Abucayon, R.L. Khade, D.R. Powell, M.J. Shaw, Y. Zhang, G.B. Richter-Addo, Over or under: Hydride attack at the metal versus the coordinated nitrosyl ligand in ferric nitrosyl porphyrins, Dalton Trans., 45 (2016) 18259-18266.

[46] M.K. Ellison, C.E. Schulz, W.R. Scheidt, Structural and electronic characterization of nitrosyl(octaethylporphinato)iron(III) perchlorate derivatives, Inorg. Chem., 39 (2000) 5102-5110.

[47] W.R. Scheidt, Y.J. Lee, Recent advances in the stereochemistry of metallotetrapyrroles, Struct. Bonding, 64 (1987) 1-70.

[48] X.H. Mu, K.M. Kadish, In situ FTIR and UV-visible spectroelectrochemical studies of iron nitrosyl porphyrins in nonaqueous media, Inorg. Chem., 27 (1988) 4720-4725.

[49] N. Xu, D.R. Powell, G.B. Richter-Addo, Nitrosylation in a crystal: Remarkable movements of iron porphyrins upon binding of nitric oxide, Angew. Chem. Int. Ed. Engl., 50 (2011) 9694-9696.

[50] W.R. Scheidt, Y.J. Lee, K. Hatano, Preparation and structural characterization of nitrosyl complexes of ferric porphyrinates. Molecular structure of aquonitrosyl(*meso*-tetraphenylporphinato)iron(III) perchlorate and nitrosyl(octaethylporphinato)iron(III) perchlorate, J. Am. Chem. Soc., 106 (1984) 3191-3198.

[51] G.-B. Yi, L. Chen, M.A. Khan, G.B. Richter-Addo, Activation of thionitrites and isoamyl nitrite by group 8 metalloporphyrins and the subsequent generation of nitrosyl thiolates and alkoxides of ruthenium and osmium Porphyrins, Inorg. Chem., 36 (1997) 3876-3885.